Phytochemistry 172 (2020) 112288

Contents lists available at ScienceDirect

Phytochemistry

journal homepage: www.elsevier.com/locate/phytochem

Chemical constituents from shells of *Xanthoceras sorbifolium*

Gang Chen[a], Yumeng Xie[a], Di Zhou[a], Yanqiu Yang[b], Jingyu Liu[b], Yue Hou[b], Maosheng Cheng[c], Yang Liu[c,**], Ning Li[a,*]

[a] School of Traditional Chinese Materia Medica, Shenyang Pharmaceutical University, Shenyang, 110016, Liaoning, China
[b] School of Life Science and Biopharmaceutics, Shenyang Pharmaceutical University, 103 Wenhua Road, Shenyang, China
[c] Key Laboratory of Structure-Based Drug Design & Discovery of Ministry of Education, School of Pharmaceutical Engineering, Shenyang Pharmaceutical University, Shenyang, 110016, China

ARTICLE INFO

Keywords:
Xanthoceras sorbifolium
Sapindaceae
Triterpene saponins
Neuroinflammation
Docking
Microglia

ABSTRACT

Three undescribed triterpenes and four previously unreported saponins, along with two known ones, were isolated from shells of *Xanthoceras sorbifolium* (Sapindaceae). Their structures were elucidated by the interpretation of 1D and 2D NMR data. The nitric oxide (NO) assay revealed that 28-*O*-isobutyryl-21-*O*-angeloyl-R_1-barrigenol and 3-*O*-*β*-D-6-*O*-methylglucuronopyranosyl-21,22-di-*O*-angeloyl-R_1-barrigenol possessed stronger inhibitory effects on LPS-induced NO overproduction (IC_{50} = 18.5 ± 1.2 and 28.2 ± 1.8 μM, respectively) than the positive drug minocycline (IC_{50} = 30.1 ± 1.3 μM) in activated BV2 cells. Western blot, RT-qPCR, and docking experiments further validated that the regulation of iNOS and IL-1β expressions was involved in the anti-neuroinflammatory effects of these two compounds.

1. Introduction

Xanthoceras sorbifolium Bunge (Sapindaceae), the nuts of which has been used to treat infantile enuresis for generations in China, is a monotypic genus of *Xanthoceras*, and was included in the pharmacopoeia (1977 edition) of China (Pharmacopoeia Committee of the People's Republic of China, 1977). Phenols from *X. sorbifolium* have been reported to display anti-tumor, radical-scavenging, and neuroinflammation-inhibiting effects (Li et al., 2016a; Yang et al., 2016). Previous chemical studies have showed that oleanene-type and barrigenol-like triterpenes are the main constituents of *X. sorbifolium*. (Wang et al., 2017; Xiao et al., 2013; Yu et al., 2012; Zhang et al., 2019). In recent years, more attention has been paid to *X. sorbifolium* due to the neuroprotective effects that it exhibits in Alzheimer Diseases (AD)-related models. The xanthoceraside from *X. sorbifolium* has been reported to elicit protective effects on $A\beta_{25-35}$-induced learning and memory impairment in mice (Chi et al., 2009). Extracts of *X. sorbifolium* also has been reported to show similar effects by attenuating dendritic spine deficiency and cognitive decline through the up-regulation of BDNF (Li et al., 2016b). A latest research has demonstrated that compared to the positive drug (huperzine A), more targets, including those related to neuroinflammation, energy metabolism and antioxidant ability, are involved in the cognitive disorder protective effects of the husk extract of *X. sorbifolium* (Rong et al., 2019). Due to the potent *in vivo* effect, the pharmaceutical research has been conducted to increase the water solubility of xanthoceraside by constructing xanthoceraside hollow gold nanoparticles aiming at promoting the bioavailability (Meng et al., 2016).

To our best knowledge, so far there is no well-acknowledged target for AD as almost all the candidate drugs failed the phase III clinical trial. However, it has been well acknowledged that neuroinflammation is a key factor in the pathogenesis of neurodegeneration in AD (Buckwalter and Wyss-Coray, 2004). In addition to the aforementioned result that anti-neuroinflammation is one of the *in vivo* mechanisms of the husk extract of *X. sorbifolium* (Rong et al., 2019), exploring more anti-neuroinflammatory constituents from *X. sorbifolium* will contribute to the discovery of natural anti-AD agents. Therefore, in this paper, the isolation and identification of seven previously undescribed (**1**–**7**) and two known triterpene compounds (**8**–**9**) from *X. sorbifolium* and their *in vitro* anti-neuroinflammatory effects in activated microglia were reported.

2. Results and discussion

2.1. Phytochemical investigation

Seven previously undescribed (**1**-**7**) and two known triterpene compounds 21-*O*-(3′,4′-di-*O*-angeloyl)-*β*-D-fucopyranosyl barrigenol C

* Corresponding author.
** Corresponding author.
E-mail addresses: y.liu@syphu.edu.cn (Y. Liu), liningsypharm@163.com (N. Li).

https://doi.org/10.1016/j.phytochem.2020.112288
Received 14 September 2019; Received in revised form 25 January 2020; Accepted 27 January 2020

(**8**) (Chen et al., 1984) and 28-*O*-acetyl-3-*O*-[*α*-L-arabinofuranosyl-(1 → 3)]-[*β*-D-galactopyranosyl-(1 → 2)]-*β*-D-6-*O*-methylglu-curonopyranosyl-21-*O*-(3′,4′-di-*O*-angeloyl)-*β*-D-fucopyranosyl barrigenol C (**9**) (Wang et al., 2016) were isolated from the 70% ethanol extract of shells of *X. sorbifolium* (see Fig. 1).

Compound **1** was obtained as a white amorphous powder, showing the pseudo-molecular ion peak m/z 685.4316 $[M-H]^-$ in the HRESI-MS spectra. Therefore, the molecular formula of **1** was determined as $C_{40}H_{62}O_9$ (calcd. 685.4340 for $C_{40}H_{61}O_9$). The ^1H NMR spectra gave seven angular methyl signals at δ_H 0.67 (Me-24), 0.80 (Me-29), 0.88 (Me-25), 0.89 (Me-26), 0.89 (Me-23), 1.00 (Me-30), and 1.30 (Me-27); one olefinic proton signal at δ_H 5.37 (1H, br s, H-12); signals of four oxygen-substituted methines at δ_H 3.63 (1H, m, H-15), 3.71 (1H, m, H-16), 5.54 (1H, d, J = 10.1 Hz, H-22), and 5.79 (1H, d, J = 10.1 Hz, H-21). Accordingly, the ^{13}C NMR spectra also revealed seven methyl signals at δ_C 15.5 (Me-25), 16.1 (Me-24), 17.0 (Me-26), 19.4 (Me-30), 20.3 (Me-27), 28.2 (Me-23), and 29.1 (Me-29), along with four oxygen-substituted methine signals at δ_C 66.3 (C-15), 72.9 (C-16), 71.5 (C-22), and 79.8 (C-21) as determined by the HSQC spectra. All these NMR data were characteristic resonances of barrigenol-like triterpenes (Wang et al., 2017). Through comparing NMR signals assignable to the triterpene skeleton with those in the literature (Wang et al., 2017), the triterpene skeleton of **1** was elucidated as R1-barrigenol (5α-olean-12-ene-3β,15α,16α,21β,22α,28-hexol). The relative configuration of the R1-barrigenol skeleton was determined based on both NOESY correlations (H-24/H-25/H-26/H-15/H-28/H-22/H-30, H-3/H-23/H-5/H-7/H-27, and H-29/H-21) (Fig. 2) and the multiplicity of H-21/22 (J = 10.1 Hz) that suggested the axial orientation for H-21 and H-22. In addition, one angeloyl and one oxyangeloyl were also deduced due to chemical shifts of [δ_C 15.5 (C-5″), 20.4 (C-4″), 127.6 (C-3″), 138.4 (C-2″), 166.1 (C-1″) for angeloyl] and [δ_C 13.1 (C-5′), 19.2 (C-4′), 58.8 (C-3′), 59.3 (C-2′), 168.7 (C-1′) for oxyangeloyl (Li et al., 2005)]. In the NOESY spectra, the correlation of δ_H 3.05 (H-3′)/δ_H 1.42 (H-5′) suggested the *cis*-configuration of H-3'/H-5'. Subsequently, HMBC correlations from δ_H 5.73 (H-21) to δ_C 168.7 (C-1′), and from δ_H 5.54 (H-22) to δ_C 166.1 (C-1″) determined the location of the angeloyl and the epoxyangeloyl (Fig. 3). Therefore, the structure of **1** was established as 21-*O*-epoxyangeloyl-22-*O*-angeloyl-R1-barrigenol.

Compound **2** was also obtained as a white amorphous powder with the molecular formula of $C_{40}H_{64}NaO_{10}$ as indicated by the pseudo-molecular ion peak m/z 727.4417 $[M+Na]^+$ (calcd. 727.4397 for $C_{40}H_{64}NaO_{10}$) in the HRESI-MS spectra. The ^1H NMR data was associated with the ^{13}C NMR data by the HSQC spectra as summarized in Tables 1 and 2. Through comparing NMR data of **1** and **2**, it was suggested that except for NMR signals of the epoxyangeloyl, all the NNR resonances of **1** ascribable to the R_1-barrigenol and angeloyl moieties were identical to those of **2** (Tables 1 and 2), indicating a different substituent linked to C-21 in **2** compared with that of **1**. The remaining carbon signals in **2** [δ_C 174.5 (C-1′), 77.4 (C-2′), 70.5 (C-3′), 21.4 (C-4′), 16.8 (C-5′)] resembled those of the 2, 3-dihydroxy-2-methylbutyryl (Torres-Valencia et al., 1998), which was further confirmed by the HMBC correlations from H-5′ to C-1'/C-3′, and from H-4′ to C-2' (Fig. 3). Finally, based on the correlation between H-21 and C-1′ in the HMBC spectrum, the structure of **2** was determined as 21-*O*-(2, 3-dihydroxy-2-methylbutyryl)-22-*O*-angeloyl-R_1-barrigenol.

Compound **3** possessed the molecular formula of $C_{39}H_{62}O_8$ determined by the pseudo-molecular ion peak m/z 681.4322 $[M+Na]^+$ (calcd. 681.4342 for $C_{39}H_{62}NaO_8$) provided by the HRESI-MS. The NMR data of **3** were quite similar to those of **1** and **2** regarding the R_1-barrigenol moiety (Tables 1 and 2), suggesting that **3** had the same triterpene skeleton as **1** and **2**. Apparent difference in the ^{13}C NMR data of **3**, compared with those of **1** and **2**, were observed at C-22 (δ_C 69.1 for **3** vs δ_C 71.5 and δ_C 71.4 for **1** and **2**, respectively) and C-28 (δ_C 63.9 for **3** vs δ_C 62.1 for both **1** and **2**), indicating different substitution patterns of C-22 and C-28 for **3**. Besides those assignable to the R_1-barrigenol moiety, one group of angeloyl [δ_C 15.4 (C-4′), 20.6 (C-5′), 128.6 (C-2′), 135.3 (C-3′), 167.3 (C-1′)] and isobutyryl [δ_C 18.7 (C-4″), 18.9 (C-3″), 33.5 (C-2″), 175.6 (C-1″)] signals were also observed. In the HMBC spectra, correlations from H-21 to C-1′ of the angeloyl, and from H-28 to C-1″ of the isobutyryl allowed the determination of the location for the angeloyl and the isobutyryl, respectively (Fig. 3). Therefore, **3** was elucidated as 28-*O*-isobutyryl-21-*O*-angeloyl-R_1-barrigenol.

Compound **4** was obtained as a white amorphous powder, and its molecular formula was elucidated to be $C_{42}H_{66}O_{13}$ as deduced by the $[M-H]^-$ *m/z*: 777.4445 (calcd. 777.4425 for $C_{42}H_{65}O_{13}$) observed in the HRESI-MS spectra. The proton signals of δ_H 4.29 (d, J = 7.8 Hz) with the corresponding carbon signal at δ_C 105.5 determined by the HSQC spectra suggested the presence of an anomeric proton of a sugar moiety in **4**. The NMR data assigned to the aglycone moiety of **4** were closely similar to those of **3**, expect for the absence of signals of the isobutyryl located at C-28 of **3** (Tables 1 and 2). And the high-field shifted C-28 carbon signal in **4** (δ_C 63.9 for **3** and δ_C 62.5 for **4**) further confirmed that the C-28 hydroxyl was unbound. In the HMBC spectra, the correlation from H-21 to C-1′ of the angeloyl group was detected (Fig. 3), leading to the determination of the aglycone of **4** as 21-*O*-angeloyl-R_1-barrigenol. Furthermore, by comparing the NMR data of the sugar moiety [δ_C 105.5 (C-1″), 73.7 (C-2″), 75.9 (C-3″), 71.7 (C-4″), 75.3 (C-

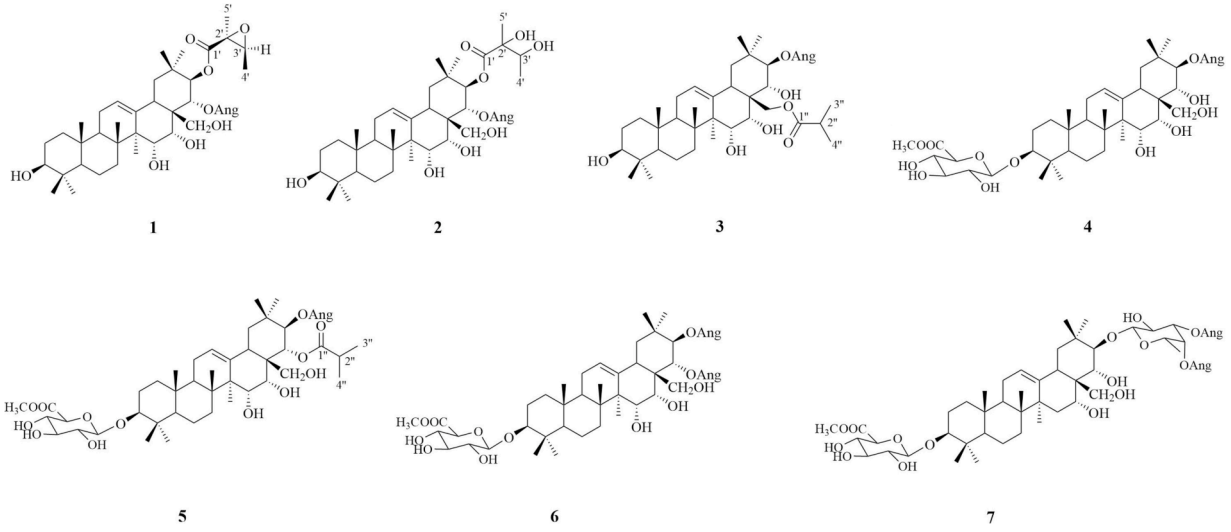

Fig. 1. Structures of previously unreported compounds 1–7 from *X. sorbifolium*. Ang: angeloyl. Ang: angeloyl.

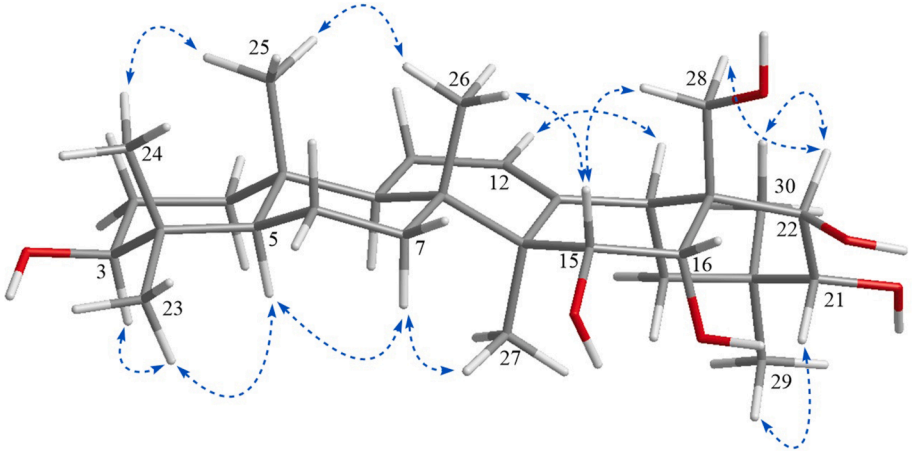

Fig. 2. Key NOE correlations of 1.

5″), 169.7 (C-6″), 51.9 (-OCH_3)] to those in the literature (Nakamura et al., 2010) and the HMBC correlation from δ_H 3.66 (-OCH_3) to δ_C 169.7 (C-6″), the *β*-D-6-*O*-methylglucuronopyranosyl was also elucidated. The absolute configuration of the sugar moiety was also determined by the hydrolysis experiment (see experimental section) of the alkaline hydrolysis-afforded product (Brenner, 2013) of **4**, which showed the presence of the D-glucuronic acid. Combined with the correlation between δ_H 4.29 (H-1″) and δ_C 88.1 (C-3) in the HMBC spectra, **4** was established as 3-*O*-*β*-D-6-*O*-methylglucuronopyranosyl-21-*O*-angeloyl-R_1-barrigenol.

Compounds **5** and **6** were both 6-*O*-methylglucuronopyranosides with 21-*O*-angeloyl-R_1-barrigenol as the triterpene skeleton as deduced through comparing the NMR data of **5** and **6** with those of **4**. In addition to the NMR signals identical to those of **4**, chemical shifts for C-22 of **5** and **6** were both δ_C 71.9, which was apparently high-field shifted compared with that of **4** (δ_C 69.7), suggesting that hydroxyls of C-22 in **5** and **6** were substituted. Additionally, NMR data of **5** afforded a group of isobutyryl signals [δ_C 175.4 (C-1″), 33.6 (C-2″), 18.7 (C-3″), and 18.9 (C-4″)], while the ^{13}C NMR spectra of **6** revealed a group of angeloyl sigals [δ_C 166.6 (C-1″), 128.2 (C-2″), 135.7 (C-3″), 15.2 (C-4″), and 20.3 (C-5″)], which were consistent with the HR-ESI MS-indicated molecular formulas of $C_{46}H_{72}NaO_{14}$ for **5** and $C_{47}H_{72}NaO_{14}$ for **6** based on the quasi-molecular ion peaks ($[M+Na]^+$ *m/z*: 871.4838 for **5**; $[M+Na]^+$ *m/z*: 883.4843 for **6**). In conjunction with HMBC correlations from δ_H 5.44 (H-22) to δ_C 175.4 (C-1″) for **5**, and from δ_H 5.54 (H-22) to δ_C 166.6 (C-1″) for **6**, the structures of **5** and **6** were determined as 3-*O*-*β*-D-6-*O*-methylglucuronopyranosyl-21-*O*-angeloyl-22-*O*-isobutyryl-R_1-barrigenol (**5**) and 3-*O*-*β*-D-6-*O*-methylglucuronopyranosyl-21,22-di-*O*-angeloyl-R_1-barrigenol (**6**), respectvely.

Compound **7** afforded the quasi-molecular ion peak of $[M+Na]^+$ m/z: 1013.5473 in the HR-ESI spectra, suggesting the molecular formula of $C_{53}H_{82}NaO_{17}$ (calcd 1013.5450 for $C_{53}H_{82}NaO_{17}$). Two sets of anomeric NMR signals were shown at δ_C 105.5 (δ_H 4.29, d, J = 7.7 Hz) and δ_C 104.4 (δ_H 4.40, d, J = 7.7 Hz), which means there were two monosaccharides in **7**. Furthermore, the NMR data of **7** indicated the presence of 3-*O*-*β*-D-6-*O*-methylglucuronopyranosyl-R_1-barrigenol moiety via comparing to NMR data of **5** and **6** (Tables 1 and 2). The remaining NMR data of **7** were identical to those of 3,4-di-*O*-angeloyl-*β*-D-fucopyranosyl in the literature (Chen et al., 1984). HMBC correlations from H-3" (δ_H 5.03) to C-1‴ (δ_C 166.3) and from H-4" (δ_H 5.23) to C-1⁗ (δ_C 166.6) further confirmed the existence of the 3,4-di-*O*-angeloyl-*β*-D-fucopyranosyl moiety. Additionally, compared with **5** and **6**, a significant low-field shift occurred at C-21 of **7** (δ_C 90.7 for **7**; δ_C 77.9 and 77.6 for **6** and **5**, respectively), indicating that the 3,4-di-*O*-angeloyl-*β*-D-fucopyranosyl was linked to C-21 of **7**. HMBC correlation from H-21 to C-1″ of the 3,4-di-*O*-angeloyl-*β*-D-fucopyranosyl confirmed the deduced linkage (Fig. 3). Therefore, **7** was elucidated as 3-*O*-*β*-D-6-*O*-methylglucuronopyranosyl-21-*O*-(3,4-di-*O*-angeloyl-*β*-D-fucopyranosyl) barrigenol C.

2.2. Inhibitory effect on LPS-activated microglia

In the central nervous system (CNS), microglia is the main resident immunocompetent and phagocytic cell, and activation of it would induce the production of neurotoxic factors, such as nitric oxide (NO) and

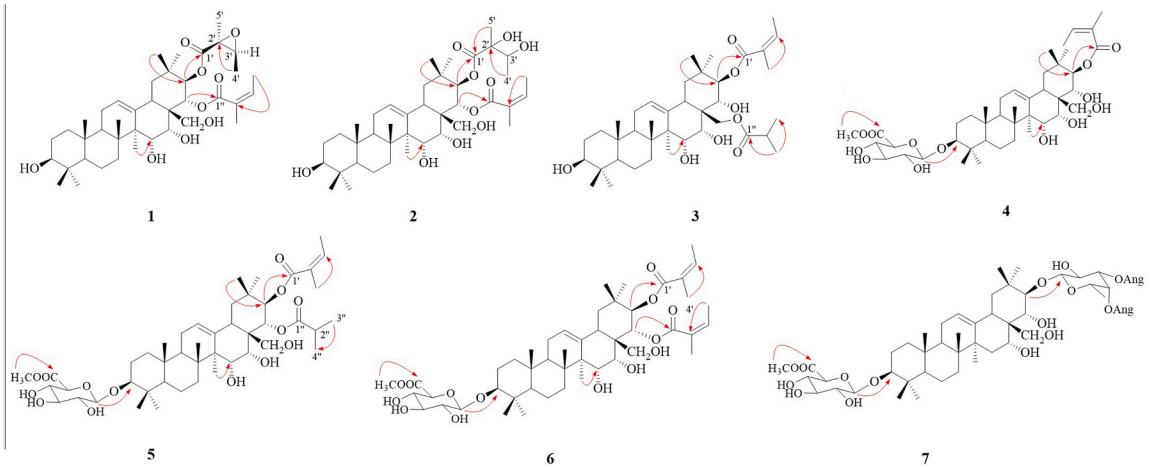

Fig. 3. Key HMBC correlations of compounds 1–7. Ang: angeloyl.

Table 1
^{1}H NMR data of 1–7 (DMSO-d_6).

No.	1	2	3	4	5	6	7
1	0.91/1.53 m	0.90/1.53 m	0.88 m/1.51 m	0.88 m/1.52 m	1.52 m/1.88 m	0.90/1.54 m	0.89 m/1.51 m
2	1.45 m	1.45 m	1.44 m	1.52 m/1.62 m	1.53 m/1.64 m	1.54 m	1.63 m
3	3.01 m	3.00 m	2.99 m	3.06 m	3.06 m	3.07 (dd, 4.3, 11.5)	3.07 (dd, 4.2, 11.3)
5	0.67 overlap	0.67 overlap	0.66 m	0.70 (d, 11.9)	0.70 (d, 11.8)	0.70 (d, 11.8)	0.72 (d, 11.8)
6	1.29 m	1.44 m	1.30/1.43 m	1.43 m	1.28 m/1.43 m	1.22 m/1.44 m	1.31 m/1.48 m
7	1.60/1.70 m	1.59/1.70 m	1.60/1.71 m	1.59 m/1.69 m	1.59 m/1.68 m	1.60 m/1.70 m	1.26 m
9	1.48 (d, 8.9)	1.47 (d, 8.6)	1.44/1.79 m	1.46 (d, 9.0)	1.47 m	1.49 m	1.56 m
11	1.83 (dd, 3.3, 8.9)	1.82 (dd, 3.4, 8.6)	1.79 m	1.80 (dd, 5.3, 9.0)	1.81 m	1.82 m	1.80 m
12	5.37 br s	5.37 br s	5.29 br s	5.35 br s	5.35 br s	5.36 br s	5.20 br s
15	3.63 m	3.62 m	3.65 m	3.60 m	3.62 m	3.63 m	1.18 (d, 9.1)/1.58 m
16	3.71 m	3.71 m	3.77 m	3.74 m	3.72 m	3.73 m	4.02 (d, 9.1)
18	2.43 m	2.43 m	2.40 (dd, 3.7, 14.4)	2.43 m	2.43 m	2.43 m	2.40 m
19	1.13 (dd, 3.1, 11.7)	1.09 overlap	1.07/2.53 m	1.05/2.43 m	1.12 m/2.52 m	1.13 m/2.53 m	0.96 m
21	5.79 (d, 10.1)	5.73 (d, 10.1)	5.56 (d, 10.0)	5.52 (d, 9.9)	5.77 (d, 10.0)	5.81 (d, 10.1)	4.03 (d, 9.4)
22	5.54 (d, 10.1)	5.52 (d, 10.1)	3.77 (d, 10.0)	3.86 (d, 9.9)	5.44 (d, 10.0)	5.54 (d, 10.1)	3.75 (d, 9.4)
23	0.89 s	0.90 s	0.90 s	0.97 s	0.97 s	0.97 s	1.89 s
24	0.67 s	0.67 s	0.67 s	0.75 s	0.75 s	0.75 s	0.83 s
25	0.88 s	0.88 s	0.87 s	0.89 s	0.88 s	0.89 s	0.88 s
26	0.89 s	0.90 s	0.90 s	0.90 s	0.89 s	0.90 s	0.75 s
27	1.30 s	1.30 s	1.28 s	1.27 s	1.30 s	1.31 s	1.35 s
28	2.87/3.09 m	2.87/3.09 m	3.80 (d, 10.6)/3.65 (d, 10.6)	2.87/3.09 m	2.87 m/3.09 m	2.90/3.12 (dd, 3.7, 10.0)	2.87/3.09 m
29	0.80 s	0.78 s	0.77 s	0.75 s	0.77 s	0.78 s	0.96 s
30	1.00 s	098 s	0.95 s	0.91 s	0.97 s	0.99 s	0.91 s
	21-	21	21-Ang	21-Ang	21-Ang	21-Ang	3-*O*-Glc A
1′	–	–	–	–	–	–	4.29 (d, 7.7)
2′	–	–	–	–	–	–	3.01 m
3′	3.05 (q, 5.4)	3.65 (q, 6.4)	6.01 (q, 7.0)	6.00 (br q, 7.2)	6.07 (br q, 7.1)	5.94 (br q, 7.1)	3.16 (d, 9.7)
4′	1.05 (d, 5.4)	0.96 (d, 6.4)	1.91 (d, 7.0)	1.91 (br d, 7.2)	1.88 (br d, 7.1)	1.85 (d,7.1)	3.30 m
5′	1.42 s	1.08 s	1.86 s	1.86 br s	1.76 br s	1.76 s	3.72 (d, 9.7)
OMe	–	–	–	–	–	–	3.66 s
	22-Ang	22-Ang	28-	3-*O*-Glc A	22-	22-Ang	21-*O*-Fuco
1″	–	–	–	4.29 (d, 7.8)	–	–	4.40 (d, 7.7)
2″	–	–	2.54 m	2.99 m	2.36 m	–	3.57 m
3″	6.10 (br q, 7.3)	6.02 (br q, 7.1)	1.09 (d, 7.0)	3.16 m	1.01 (d,7.0)	6.00 (dq, 7.1)	5.03 (dd, 3.5, 10.1)
4″	1.92 (d, 7.1)	1.90 (d, 7.1)	1.10 (d, 7.0)	3.28 m	0.96 (d,7.0)	1.81 (dd, 7.1)	5.23 (d, 3.5)
5″	1.78 br s	1.79 br s	–	3.72 m	–	1.76 s	4.08 m
6″	–	–	–	–	–	–	1.04 (d, 6.3)
OMe	–	–	–	3.66 s	–	–	–
					3-*O*-Glc A	3-*O*-Glc A	3″-*O*-Ang
1‴					4.29 (d, 7.7)	4.29 (d,7.8)	–
2‴					3.00 m	3.01 m	–
3‴					3.16 m	3.17 m	6.10 (q, 7.2)
4‴					3.28 m	3.30 m	1.91(d, 7.2)
5‴					3.72 m	3.73 m	1.75 br s
OMe					3.66 s	3.66 s	–
							4″-*O*-Ang
3‴′							6.20 (q, 7.3)
4‴′							1.88 (d, 7.3)
5‴′							1.86 br s

IL-1β, that mediates inflammatory processes in CNS. Moreover, the activated microglia has also been indicated in pathological lesions in neurological diseases. Thus, examining the NO production in LPS-treated microglia has been used as a *in vitro* model to screen the anti-neuroinflammtory agents (Li et al., 2015; Wu et al., 2007).

In this paper, all these nine isolates (**1–9**) were subjected to the *in vitro* evaluation on the NO production in LPS-activated BV2 cells. Though **1–9** are structurally similar, only compounds **3** and **6** exhibited potent inhibitory effects (IC_{50} = 18.5 ± 1.2 and 28.2 ± 1.8 μM for **3** and **6**, respectively) (Fig. 4) compared with the positive drug minocycline (IC_{50} = 30.1 ± 1.3 μM), while the remaining compounds showed no effects (IC_{50} > 100 μM). To further understand the effect of **3** and **6**, the inducible nitric oxide synthase (iNOS) and IL-1β expression were tested via Western blot and RT-qPCR methods. The results showed that both **3** and **6** potently suppressed the LPS-induced ectopic up-regulation of iNOS (Fig. 5A) and IL-1β (Fig. 5B), suggesting the anti-neuroinflammatory effects of **3** and **6**.

Moreover, inhibitory effects on iNOS of **1–3** were also investigated through docking study for these three aglycones elicited different effects on NO production. The software of Glide was used to examine the binding ability of **1–3** to the protein iNOS (PDB:4UX6). The docking results showed that **3** perfectly occupied the active pocket of iNOS (Fig. 6A–C), while **1** and **2** failed to dock into the same site on iNOS, being consistent with the *in vitro* result of the NO assay.

Table 2
^{13}C NMR data of 1–7 (DMSO-d_6).

No.	1	2	3	4	5	6	7
1	38.5	38.4	38.5	38.4	38.4	38.4	38.2
2	27.1	27.1	27.1	25.7	25.7	25.7	25.7
3	76.8	76.8	76.8	88.1	88.1	88.1	88.1
4	38.3	38.3	38.3	38.7	38.7	38.7	38.6
5	54.6	54.6	54.6	54.7	54.7	54.7	54.9
6	18.2	18.2	18.2	18.0	18.0	18.0	17.8
7	35.6	35.7	35.7	35.6	35.6	35.6	32.3
8	40.6	40.6	40.5	40.5	40.6	40.6	39.5
9	46.3	46.3	46.2	46.3	46.2	46.2	46.1
10	36.2	36.6	36.6	36.3	36.3	36.3	36.2
11	23.1	23.1	23.2	23.1	23.1	23.1	23.0
12	124.6	124.5	124.5	123.9	124.4	124.5	122.1
13	142.5	142.6	142.5	143.3	142.6	142.6	142.9
14	46.6	46.6	46.8	46.5	46.6	46.7	40.8
15	66.3	66.4	66.4	66.3	66.2	66.3	33.5
16	72.9	72.9	71.3	71.8	72.2	72.8	67.0
17	46.9	46.8	46.4	46.6	46.6	46.6	46.4
18	39.8	39.8	40.2	39.7	39.4	39.4	38.6
19	46.0	46.2	45.9	46.7	46.0	46.1	47.3
20	35.6	35.8	35.2	35.3	35.4	35.4	36.2
21	79.8	78.6	79.7	80.2	77.6	77.9	90.7
22	71.5	71.4	69.1	69.7	71.9	71.9	69.8
23	28.2	28.2	28.3	27.5	27.5	27.5	27.5
24	16.1	16.1	16.1	16.5	16.5	16.5	16.4
25	15.5	15.5	15.5	15.4	15.5	15.5	15.6
26	17.0	17.0	17.0	17.0	17.0	17.0	16.5
27	20.3	20.3	20.2	20.2	20.3	20.3	26.8
28	62.1	62.1	63.9	62.5	62.3	62.1	63.0
29	29.1	29.1	29.3	29.4	29.0	29.0	29.2
30	19.4	19.4	19.6	19.7	19.6	19.5	19.7
	21-	21-	21-Ang	21-Ang	21-Ang	21-Ang	3-*O*-Glc A
1′	168.7	174.5	167.3	167.4	166.4	166.5	105.5
2′	59.3	77.4	128.6	128.6	127.6	127.8	73.6
3′	58.8	70.5	135.4	135.3	137.5	136.7	75.9
4′	13.1	21.4	15.4	15.5	15.4	15.3	71.6
5′	19.2	16.8	20.6	20.6	20.4	20.3	75.3
6′	–	–	–	–			169.7
OMe	–	–	–	–			51.8
	22-Ang	22-Ang	28-	3-*O*-Glc A	22-	22-Ang	21-*O*-Fuco
1″	166.1	166.5	175.6	105.5	175.4	166.6	104.4
2″	127.6	127.9	33.5	73.7	33.6	128.2	68.8
3″	138.4	137.4	18.9	75.9	18.7	135.7	72.9
4″	15.5	15.5	18.7	71.7	18.9	15.2	70.3
5″	20.4	20.5	–	75.3	–	20.3	68.1
6″	–	–	–	169.7	–	–	15.9
OMe	–	–	–	51.9	–	–	–
					3-*O*-Glc A	3-*O*-Glc A	3″-*O*-Ang
1‴					105.5	105.5	166.3
2‴					73.7	73.7	127.2
3‴					75.9	75.9	137.9
4‴					71.7	71.7	15.4
5‴					75.3	75.3	19.9
6‴					169.7	169.7	–
OMe					51.9	51.8	–
							4″-*O*-Ang
1⁗							166.6
2⁗							126.9
3⁗							138.3
4⁗							15.4
5⁗							20.3

3. Conclusion

Three undescribed triterpenes (**1–3**) and four previously unreported saponins (**4–7**), along with two known ones (**8–9**), were isolated from *X. sorbifolium*. The NO assay revealed that **3** and **6** possessed stronger inhibitory effects on LPS-induced NO overproduction than the positive drug minocycline in activated BV2 cells. The anti-neuroinflammtory effects of **3** and **6** were also confirmed by the Western blot, RT-qPCR,

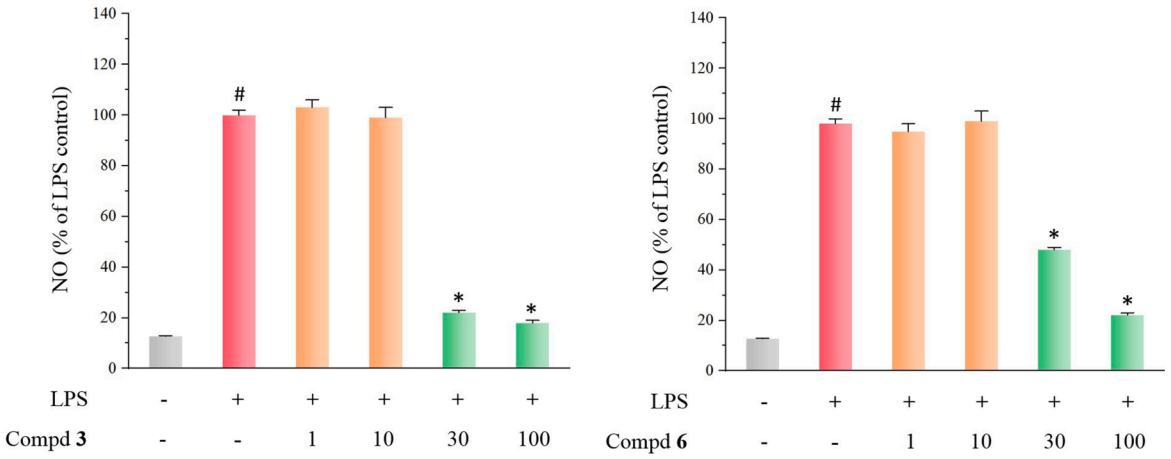

Fig. 4. Inhibitory effects of compounds 3 and 6 on NO production in LPS-activated BV2 cells. Values are means ± S.E.M. from three separate experiments and are normalized to the control group. ($^{\#}P < 0.05$ compared with the control group; $^{*}P < 0.05$ compared with the LPS group).

and docking experiments, and the results of which showed that both iNOS and IL-1β expressions were repressed by **3** and **6** in LPS-activated BV2 cells, which might suggested great potentials for **3** and **6** in the therapy of neurodegenerative diseases such as AD.

4. Experimental

4.1. Chemistry

NMR spectra were recorded on Bruker ARX-400 and 600 M AVIII spectrometers, using TMS as an internal standard. HRESI-MS was acquired on a Bruker micro TOF-Q mass spectrometer in m/z mode. Silica gel (200–300 mesh) for chromatography was produced by Qingdao Ocean Chemical Group Company (Qingdao, China). ODS (50 μm) was afforded by YMC Company (Ltd) (Japan). HPLC separations were performed on a YMC-pack Prep-ODS column (250 × 20 mm) equipped with a Shimadzu RID-20AUV detector and a Shimadzu LC-6AD series pumping system (Tokyo, Japan). Pyridine-d_5 were obtained from Sigma-Aldrich Company (St. Louis, USA). All the chromatographic and analytical grade reagents were obtained from Tianjin DaMao Chemical Company (Tianjin, China).

4.2. Plant material

The shell of Xanthoceras sorbifolium Bunge (Sapindaceae) was collected in Fuxin city (N42.081°, E121.403°), Liaoning province in September (autumn), 2018. The Shells of *X. sorbifolium* was prepared by removing the kernel and the flesh of the fruits. The material was identified by Professor Yingni Pan (School of Traditional Chinese Materia Medica, Shenyang Pharmaceutical University). A voucher specimen (No.20180921) is deposited in School of Traditional Chinese Materia Medica, Shenyang Pharmaceutical University.

4.4. Acid hydrolysis

For compounds **4–7** (each 2.0 mg), an alkaline hydrolysis experiment (Brenner, 2013) was performed to remove the methyl group in sugars (dissolved in 1.5 ml 5% KOH:Dioxane 1.5 ml, stirred at 37 °C for 1 h). The powder afforded by the alkaline hydrolysis was dissolved in 4 M HCl (2 mL) and then heated in a H_2O bath at 90 °C for 3 h to dryness. Mixture was extracted by CH_2Cl_2 and get CH_2Cl_2 extract. The water layer was identified using GC method by treating the residue with L-cysteine methyl ester hydrochloride (0.01 ml) in pyridine (0.02 ml) at 60 °C for 1 h. After this reaction, the solution was treated with *N,O*-bis (trimethyl silyl) trifluoroacetamide (0.01 ml) at 60 °C for 1 h. Column: Supelco STBTM-1 (30 m × 0.25 mmi.d.). Injetor temp.:230. Detector temp: 230 °C. Column temp.:230. He flow rate: 15 ml/min (methyl-D-glucuronic acid: 20.16 min). Additonally, residues were analyzed by HPLC with an NH2P-50 4 E column (4.6 × 250 mm, Showa Denko K.K., Japan) and an optical rotation detec-tor (JASCO ORD-4090, JASCO International Co, Ltd., Japan) to detect the configuration of the fucose

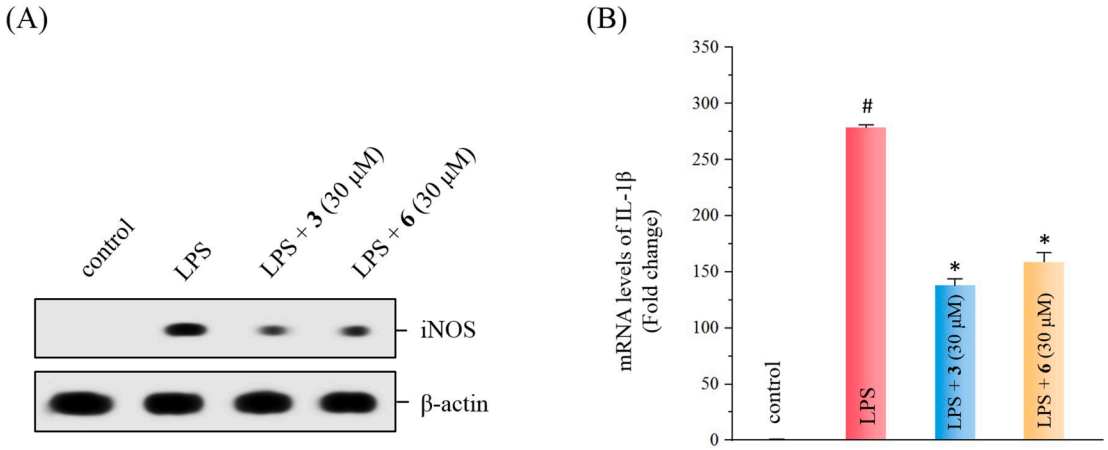

Fig. 5. Effects of compounds 3 and 6 on iNOS and IL-1β expressions in LPS-activated BV2 cells. (A) Representative Western blot result of 3 and 6 attenuating iNOS expression. (B) RT-qPCR results of 3 and 6 suppressing IL-1β expressions. Values are means ± S.E.M. from three separate experiments and are normalized to the control group. ($^{\#}P < 0.05$ compared with the control group; $^{*}P < 0.05$ compared with the LPS group).

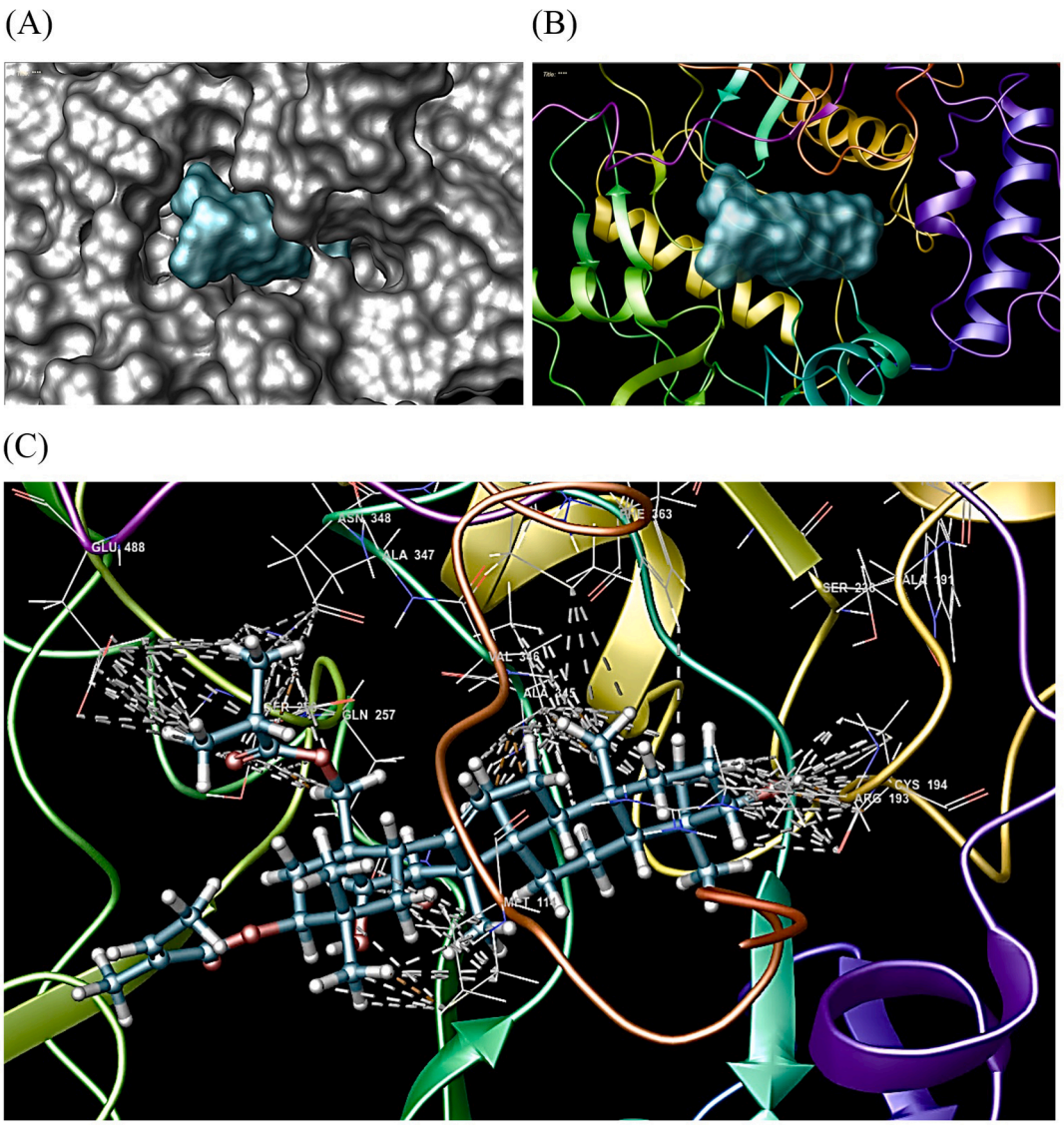

Fig. 6. Docking results by Glide showing 3 perfectly docked into the active pocket of iNOS protein (PDB:4UX6). (A) The docking result of 3 bound to the active pocket of iNOS. The iNOS protein was represented as gray solid cartoons of solid surfaces while 3 was represented as cyan solid cartoons of solid surfaces. (B) The result of (A) with iNOS represented as color ribbons. (C) The result of (A) with good contacts between 3 and iNOS represented as white short lines (3 was shown in cyan color).

using standard samples with the following condition: acetonitrile-water (75:25, v/v); flow rate, 0.8 mL/min. D-fucose, 9.5 min (positive).

4.3. Extraction and isolation

The shell of *X. sorbifolium* (200 kg) were extracted with 70% ethanol (2000 L each) under reflux for 3 × 2 h. The filtrate was concentrated under reduced pressure, and afforded the crude extract (20 kg). Ethanol extract (20 kg) was fractioned on macroporous absorptive resin (D101) column, eluting with H_2O, 20% ethanol/H_2O (Fr. A, 1255 g), 50% ethanol/H_2O (Fr. B, 2055 g), 70% ethanol/H_2O (Fr. C, 1750 g), 90% ethanol/H_2O (Fr. D, 500 g), successively. Fr. C (1750 g) was chromatographed on silica gel, eluting with CH_2Cl_2–MeOH (0:100–100:0), to give six fractions (Fr. D1-D7). Fr. D3 (20.5 g) was subjected to a ODS column washing with MeOH/H_2O (0: 100-100: 0) to get five fractions. The sub-fraction D3-2 (510 mg) was isolated by HPLC with MeOH/H_2O (80: 20) as eluent to afford compounds **1** (5.8 mg), **2** (13.5 mg), **3** (3.1 mg); sub-fraction D3-3 was isolated by HPLC with MeOH/H_2O (75: 25) as eluent to afford compounds **4** (6.5 mg), **5** (8.7 mg), **6** (11.2 mg), **7** (12.4 mg), **8** (16.1 mg); sub-fraction D3-4 (205 mg) was isolated by HPLC with MeOH/H_2O (75: 25) as eluent to afford compound **9** (4.1 mg).

21-*O*-epoxyangeloyl-22-*O*-angeloyl-R_1-barrigenol (**1**): [α] + 31.0 (c = 0.33, MeOH). UV (MeOH) λ_{max} 210 and 225 nm. IR(KBr) ν_{max} 3420, 2920, 1722, 1687, 1088 cm^{-1}. HR-ESI-MS m/z: 685.4316 $[M\text{-}H]^-$ (calcd. 685.4340 for $C_{40}H_{61}O_9$). ^1H and ^{13}C NMR data: see Tables 1 and 2

21-*O*-(2, 3-dihydroxy-2-methylbutyryl)-22-*O*-angeloyl-R_1-barrigenol (**2**): [α] + 42.0 (c = 0.43, MeOH). UV (MeOH) λ_{max} 210 and 225 nm. IR(KBr) ν_{max} 3425, 2921, 1725, 1680, 1058 cm^{-1}. HR-ESI-MS m/z: 727.4417 $[M+Na]^+$ (calcd. 727.4397 for $C_{40}H_{64}NaO_{10}$). ^1H and ^{13}C NMR data: see Tables 1 and 2

28-*O*-isobutyryl-21-*O*-angeloyl-R_1-barrigenol (**3**): [α] + 22.0 (c = 0.30, MeOH). UV (MeOH) λ_{max} 210 and 225 nm. IR(KBr) ν_{max} 3418, 2920, 1735, 1685, 1018 cm^{-1}. HR-ESI-MS m/z: 681.4322 $[M+Na]^+$ (calcd. 681.4342 for $C_{39}H_{62}NaO_8$). ^1H and ^{13}C NMR data: see Tables 1 and 2

3-*O*-β-D-6-*O*-methylglucuronopyranosyl-21-*O*-angeloyl-R_1-barrigenol (**4**): [α] + 52.0 (c = 0.55, MeOH). UV (MeOH) λ_{max} 210 and 225 nm. IR(KBr) ν_{max} 3423, 2950, 1725, 1675, 1008 cm^{-1}. HR-ESI-MS

m/z: 777.4445 [M-H]$^-$ (calcd. 777.4425 for $C_{42}H_{65}O_{13}$). ^{1}H and ^{13}C NMR data: see Tables 1 and 2

3-*O*-*β*-D-6-*O*-methylglucuronopyranosyl-21-*O*-angeloyl-22-*O*-isobutyryl-R_1-barrigenol (**5**): [*α*] + 35.0 (*c* = 0.23, MeOH). UV (MeOH) λ_{max} 210 and 225 nm. IR(KBr) ν_{max} 3425, 2910, 1725, 1680, 1015 cm^{-1}. HR-ESI-MS *m/z*: 871.4838 [M + Na]$^+$ (calcd. 871.4820 for $C_{46}H_{72}NaO_{14}$). ^{1}H and ^{13}C NMR data: see Tables 1 and 2

3-*O*-*β*-D-6-*O*-methylglucuronopyranosyl-21,22-di-*O*-angeloyl-R_1-barrigenol (**6**): [*α*] + 41.0 (*c* = 0.43, MeOH). UV (MeOH) λ_{max} 210 and 225 nm. IR(KBr) ν_{max} 3421, 2915, 1721, 1685, 1019 cm^{-1}. HR-ESI-MS *m/z*: 883.4843 [M + Na]$^+$ (calcd. 883.4820 for $C_{47}H_{72}NaO_{14}$). ^{1}H and ^{13}C NMR data: see Tables 1 and 2

3-*O*-*β*-D-6-*O*-methylglucuronopyranosyl-21-*O*-(3,4-di-*O*-angeloyl-*β*-D-fucopyranosyl) barrigenol C (**7**): [*α*] + 45.0 (*c* = 0.21, MeOH). UV (MeOH) λ_{max} 210 and 225 nm. IR(KBr) ν_{max} 3425, 2910, 1725, 1681, 1010 cm^{-1}. HR-ESI-MS *m/z*: 1013.5473 [M + Na]$^+$ (calcd. 1013.5450 for $C_{53}H_{82}NaO_{17}$). ^{1}H and ^{13}C NMR data: see Tables 1 and 2

4.5. Cell culture and in vitro evaluation of NO production

BV2 cells were cultured in Dulbecco's modified Eagle's medium (DMEM) supplemented with 10% heat-inactivated FBS in a humidified environment with 5% CO_2 at 37 °C. The measurement of NO production was conducted as previously reported (Li et al., 2015). Briefly, accumulation of nitrite (NO_2^-), an indicator of NO synthase activity, in culture medium was measured using the Griess reaction. Cells (5×10^4 cells/well) were plated on 96-well microliter plates and treated with each compound (0.1, 1, 10, 50 μM) in presence of bacterial lipopolysacchride (LPS; 100 ng/ml) for 24 h. Fifty microliter culture medium supernatants were mixed with 50 μl Griess reagent (part I: 1% sulfanilamide; part II: 0.1% naphthylethylene diamide dihydrochloride and 2% phosphoric acid) at room temperature. Fifteen minutes later, the absorbance was measured at 540 nm.

4.6. Western blot analysis

The Western blot experiment was performed with the previously reported method (Chen et al., 2019). Briefly, Whole-cell lysates were prepared using 2% SDS, sonicated and centrifuged (15,000 *g*) at 4 °C for 15 min. The supernatants were boiled for 5 min and size-fractionated by SDS/PAGE (10% acrylamide). After transferring proteins on to nitrocellulose filters, the blots were incubated with primary antibodies recognizing iNOS and GPADH (1:1000, Cell Signaling Technology, Beverly, MA) for 2 h at room temperature; following incubation with secondary antibodies for 1 h at room temperature, immunocomplexes were developed by using chemiluminescence.

4.7. Reverse transcription (RT) and quantitative real-time PCR analyses

The RT-qPCR experiment was performed as previously described (Deng et al., 2019). Total RNA from BV2 cells was extracted Trizol according to the manufacturer's instructions. Reverse transcription was carried out to obtain cDNA using the Master Mix kit (Takara, Shiga, Japan) following standard protocols. The mRNA levels of IL-1β were assessed sing a Step One Plus real-time PCR system (BIO-RAD, CFX96TM Real-time System, C1000TM Thermal Cycle, USA). For IL-1β mRNA quantification: the following sense and antisense primers were used: forward primer 5′-ATGGCAACTGTTCCTGAACTCAACT-3′, reverse primer 5′- AGGACAGGTATAG ATTCTTTCCTT-3'.

4.8. Docking studies

The docking studies were conducted with Grid-based Ligand Docking with Energetics (Glide) provided in the Schrodinger 2013 package suit as previously reported (Chen et al., 2017; Zhou et al., 2019). The three-dimensional crystal structure of iNOS (PDB ID: 4UX6) was retrieved from the Protein Databank Bank (http://www.rcsb.org/). Before docking, the preparations of proteins and ligands (**1–3**) were performed following the standard protocol of the Protein Preparation and Ligprep Wizards, respectively, of the Schrodinger 2013 Suite. Docking studies were implemented via Glide method in XP (Extra-Precision) mode.

4.9. Statistics

IC_{50}, inhibitory rate, and RT-qPCR values are means ± S.E.M. from five samples. The significance of the difference between means was determined by ANOVA. The level of significance was determined by using Duncan's multiple-range test.

Declaration of competing interest

The authors declare no competing financial interests.

Acknowledgements

This work was supported partially by the National Natural Science Foundation of China (81872768, 81673323, U1903122, U1603125), LiaoNing Revitalization Talents Program (XLYC1807118), LiaoNing BaiQianWan Talents Program (2018), Program for Liaoning Innovative Talents in University (LR2017043) and the Fundamental Research Funds for the Central Universities of China (N182008004, N182006001). Overseas Training Project of Liaoning Colleges and Universities (2018LNGXGJWPY-YB024).

References

Brenner, D.A., 2013. Reversibility of liver fibrosis. Gastroenterol. Hepatol. 9, 737–739.
Buckwalter, M.S., Wyss-Coray, T., 2004. Modelling neuroinflammatory phenotypes in vivo. J. Neuroinflammation 1, 10.
Chen, G., Han, Y., Feng, Y., Wang, A., Li, X., Deng, S., Zhang, L., Xiao, J., Li, Y., Li, N., 2019. Extract of Ilex rotunda Thunb alleviates experimental colitis-associated cancer via suppressing inflammation-induced miR-31-5p/YAP overexpression. Phytomedicine 62, 152941.
Chen, G., Zhou, D., Li, X.Z., Jiang, Z., Tan, C., Wei, X.Y., Ling, J., Jing, J., Liu, F., Li, N., 2017. A natural chalcone induces apoptosis in lung cancer cells: 3D-QSAR, docking and an in vivo/vitro assay. Sci. Rep. 7, 10729.
Chen, Y.J., Takeda, T., Ogihara, Y., Iitaka, Y., 1984. Studies on the constituents of Xanthoceras sorbifolia Bunge. II. Major sapogenol and a prosapogenin from the fruits of Xanthoceras sorbifolia Bunge. Chem. Pharm. Bull. (Tokyo) 32, 3378–3383.
Chi, T.Y., Wang, L.H., Qu, C., Yang, B.Z., Ji, X.F., Wang, Y., Okuyama, T., Yoshihito, O., Zou, L.B., 2009. Protective effects of xanthoceraside on learning and memory impairment induced by Abeta(25-35) in mice. J. Asian Nat. Prod. Res. 11, 1019–1027.
Deng, S., Wang, A., Chen, X., Du, Q., Wu, Y., Chen, G., Guo, W., Li, Y., 2019. HBD inhibits the development of colitis-associated cancer in mice via the IL-6R/STAT3 signaling pathway. Int. J. Mol. Sci. 20.
Li, J., Jiang, Z., Li, X., Hou, Y., Liu, F., Li, N., Liu, X., Yang, L., Chen, G., 2015. Natural therapeutic agents for neurodegenerative diseases from a traditional herbal medicine Pongamia pinnata (L.) Pierre. Bioorg. Med. Chem. Lett 25, 53–58.
Li, N., Wang, Y., Li, X., Zhang, H., Zhou, D., Wang, W., Li, W., Zhang, X., Li, X., Hou, Y., Meng, D., 2016a. Bioactive phenols as potential neuroinflammation inhibitors from the leaves of Xanthoceras sorbifolia Bunge. Bioorg. Med. Chem. Lett 26, 5018–5023.
Li, Y., Xu, J., Xu, P., Song, S., Liu, P., Chi, T., Ji, X., Jin, G., Qiu, S., Hou, Y., Zheng, C., Wang, L., Meng, D., Zou, L., 2016b. Xanthoceras sorbifolia extracts ameliorate dendritic spine deficiency and cognitive decline via upregulation of BDNF expression in a rat model of Alzheimer's disease. Neurosci. Lett. 629, 208–214.
Li, Z.L., Li, X., Li, L.H., Li, N., Yu, M., Meng, D.L., 2005. Two new triterpenes from the husks of Xanthoceras sorbifolia. Planta Med. 71, 1068–1070.
Meng, D.L., Shang, L., Feng, X.H., Huang, X.F., Che, X., 2016. Xanthoceraside hollow gold nanoparticles, green pharmaceutics preparation for poorly water-soluble natural anti-AD medicine. Int. J. Pharm. 506, 184–190.
Nakamura, S., Chen, G., Nakashima, S., Matsuda, H., Pei, Y., Yoshikawa, M., 2010. Brazilian natural medicines. IV. New noroleanane-type triterpene and ecdysterone-type sterol glycosides and melanogenesis inhibitors from the roots of pfaffia glomerata. Chem. Pharm. Bull. (Tokyo) 58, 90–695.
Rong, W., Ding, K., Guo, S., Xie, F., Li, Q., Bi, K., 2019. Metabolomics analysis of Xanthoceras sorbifolia husks protection of rats against Alzheimer's disease using liquid chromatography mass spectrometry. J. Chromatogr. B Analyt. Technol. Biomed. Life Sci. 1126–1127, 121739.
Torres-Valencia, J.M., Cerda-García-Rojas, C.M., Joseph-Nathan, P., 1998. Enantioselective preparation of (2R,3R)-(+)- and (2S,3S)-(−)-2,3-epoxy-2-methylbutanoic acids and some derivatives. Tetrahedron: Asymmetry 9, 757–764.

Wang, D., Dan, S., Li, X., Dan, L., Xi, R., Gao, H., Wang, X.J.R.A., 2016. Barrigenol triterpenes from the husks of Xanthoceras sorbifolia Bunge and their antitumor activities. 6, 27434–27446.
Wang, D., Su, D., Yu, B., Chen, C., Cheng, L., Li, X., Xi, R., Gao, H., Wang, X., 2017. Novel anti-tumour barringenol-like triterpenoids from the husks of Xanthoceras sorbifolia Bunge and their three dimensional quantitative structure activity relationships analysis. Fitoterapia 116, 51–60.
Wu, C.F., Bi, X.L., Yang, J.Y., Zhan, J.Y., Dong, Y.X., Wang, J.H., Wang, J.M., Zhang, R., Li, X., 2007. Differential effects of ginsenosides on NO and TNF-α production by LPS-activated N9 microglia. Int. Immunopharm. 7, 313–320.
Xiao, W., Wang, Y., Zhang, P., Li, N., Jiang, S., Wang, J.H., Huang, J., Li, X., 2013. Bioactive barrigenol type triterpenoids from the leaves of Xanthoceras sorbifolia Bunge. Eur. J. Med. Chem. 60, 263–270.
Yang, C.Y., Ha, W., Lin, Y., Jiang, K., Yang, J.L., Shi, Y.P., 2016. Polyphenols isolated from Xanthoceras sorbifolia husks and their anti-tumor and radical-scavenging activities. Molecules 21.
Yu, L., Tang, X., Chen, L., Wang, M., Jian, J., Cao, S., Wang, X., Kang, N., Qiu, F., 2012. Oleanane-type triterpenoid saponins from Xanthoceras sorbifolia Bunge. Fitoterapia 83, 1636–1642.
Zhang, X., Zhang, S., Yang, Y., Wang, D., Gao, H., 2019. Natural barrigenol-like triterpenoids: a comprehensive review of their contributions to medicinal chemistry. Phytochemistry 161, 41–74.
Zhou, D., Li, X., Chang, W., Han, Y., Liu, B., Chen, G., Li, N., 2019. Antiproliferative steroidal glycosides from rhizomes of Polygonatum sibiricum. Phytochemistry 164, 172–183.